

# An improved analysis of semiconductor laser dynamics under strong optical feedback

メタデータ	言語: eng 出版者: 公開日: 2017-10-03 キーワード (Ja): キーワード (En): 作成者: メールアドレス: 所属:
URL	<a href="http://hdl.handle.net/2297/1814">http://hdl.handle.net/2297/1814</a>

# An Improved Analysis of Semiconductor Laser Dynamics Under Strong Optical Feedback

Salah G. Abdulrhmann, *Student Member, IEEE*, Moustafa Ahmed, *Member, IEEE*, Takaharu Okamoto, Wataro Ishimori, and Minoru Yamada, *Member, IEEE*

**Abstract**—We present an improved theoretical model to analyze dynamics and operation of semiconductor lasers under optical feedback (OFB). The model is applicable for arbitrary strength of OFB ranging from weak to very strong. The model has been applied to investigate the dynamics and operation of lasers over wide ranges of OFB and injection current. An improved set of modified rate equations of lasers operating under OFB were proposed. We introduced a theoretical model to determine the power emitted from both the laser back facet and external reflector. The results showed that the operation of semiconductor lasers is classified into continuous wave, chaotic, and pulsing operations, depending on the operating conditions. The light versus current characteristics were examined in the operating regions of the classified operations. Under strong OFB, we predicted for the first time pulsing operation of lasers at injection currents well above the threshold. We observed the pulsing operation in experiments in good correspondence with the simulated results.

**Index Terms**—Chaos, external cavity, optical feedback (OFB), pulsation, semiconductor lasers, time delay.

## I. INTRODUCTION

IN MANY applications, such as optical data recording and fiber optic communication systems, semiconductor lasers operate in the presence of external optical feedback (OFB). It has been observed that even a small amount of OFB can affect the laser behavior [1]–[8]. Although the OFB may cause strong instabilities in the laser operation in forms of chaos [8], coherence collapse [3], and bistability [9], [10], it has been used for linewidth narrowing [11], [12], mode stabilization [13], and reduction of modulation-induced frequency chirp [14]. Therefore, operation of semiconductor lasers under OFB has been the subject of many theoretical investigations [15]–[18]. The behavior of semiconductor lasers under OFB is theoretically described by the coupled rate equations of the electric field and the injected carrier number. Most previous models dealing with OFB were applicable under either weak or moderate OFB and simply incorporated the OFB by adding a time-delayed feedback term in a form of linearized approximation to the standard laser rate equations [19], [20].

In applications such as power sources for fiber amplifiers in optic fiber communications, the semiconductor lasers are used with an external cavity which consists of an optical fiber and a fiber Bragg grating (FBG) in order to increase the optical power and to select the lasing wavelength. Since these pumping lasers are designed to have small reflectivity at the front facet and to be subjected to rather larger reflectivity at the FBG, the lasers suffer very strong OFB into the laser cavity [21], [22]. However, these lasers happen to show dramatic changes of the output power, lasing spectrum, and the laser dynamics [23], [24], which can degrade the device performance. A profound understanding of dynamics and operation of semiconductor lasers in this regime of strong OFB are indispensable in order to avoid the instabilities or to stabilize and control the semiconductor lasers emission.

To get reliable analysis of semiconductor lasers under an arbitrary amount of OFB, including the regime of strong OFB, we should count the OFB as time delay of the laser light [25]. This means that the round trips of the laser light in the external cavity are counted as time delays of the laser light at the front facet. Such a technique requires careful consideration of the transmission- and reflection-induced phase changes of the lasing field through the round trips in both the laser cavity and the external cavity. Moreover, numerical analysis of the time-delayed rate equations of lasers is required. Rong-Qing and Shang-Ping [26] and Langley *et al.* [27] reported improved models to analyze laser operation under strong OFB. Although the treatment in [26] is effective for the strong OFB range, the field amplitude and phase were approximated as random variables in stationary stochastic processes, which is valid if the laser dynamics are stabilized. Such approximation is not generally true, since the laser dynamics are stabilized after times much longer than the delay time  $\tau$ . Moreover, application of such a model was limited to stationary analysis of operation under OFB, which is not enough to trace the phenomena in a trustworthy fashion. Although Langley *et al.* [27] improved the Lang and Kobayashi model [15] by counting multiple reflections between the laser front facet and external mirrors, their model is still not applicable for the case of strong OFB. Moreover, the analysis in [27] was concerned only with the regime of transitions from moderate OFB-induced coherence collapse to continuous wave (CW) operation under stronger OFB.

In this paper, we propose an improved time-delay model of semiconductor lasers under OFB, which can be applicable under an arbitrary amount of OFB. The model in [15] that was commonly used to analyze laser operation under OFB is derived from our model, following appropriate approximations. We in-

Manuscript received October 1, 2002; revised August 7, 2003.

S. G. Abdulrhmann, W. Ishimori, and M. Yamada are with the Electrical and Electronic Engineering Department, Faculty of Engineering, Kanazawa University, Kanazawa 920-8667, Japan (e-mail: 5502abdu@ec.t.kanazawa-u.ac.jp; ishimori@popto5.ec.t.kanazawa-u.ac.jp; myamada@t.kanazawa-u.ac.jp).

M. Ahmed is with the Physics Department, Faculty of Science, Minia University, 61519 El-Minia, Egypt (e-mail: m.farghal@link.net).

T. Okamoto is with NTT DATA, Fujima-chi 4-26-1, Tokyo, Japan (e-mail: cbe21600@pop06.odn.ne.jp).

Digital Object Identifier 10.1109/JSTQE.2003.819500

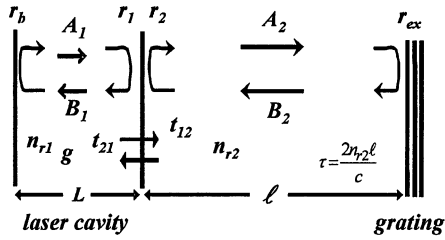


Fig. 1. Schematic illustration of a time-delay model of semiconductor lasers under OFB.

introduce new theoretical analysis to calculate the power emitted from the laser back facet as well as from the external mirror, which enables detection of laser output from both sides of the system. The present model is applied to investigate the influence of strong OFB on the dynamics and operation of semiconductor lasers. We also demonstrate classification of laser operation over wide ranges of the OFB and injection current, which presents new detailed characterization of laser operation in the strong OFB regime. The analysis indicates that the laser exhibits CW, chaos, and pulsing operation, depending on the operating conditions. The pulsing operation is theoretically predicted to characterize the strong OFB regime. We also confirm these predictions in experiments on 980-nm InGaAs lasers.

This paper is organized as follows. In the next section, we introduce a new unified model of OFB in semiconductor lasers and present new modified time-delay rate equations. We also present a new technique to calculate the power emitted from both the back facet and the external mirror. In Section III, we explain the procedures of numerical simulation. In Section IV, we present the simulated results under wide ranges of the injection current and OFB, giving special attention to the regime of strong OFB. Experimental setup and observation results under strong OFB are given in Section V. Conclusions of this paper are given in Section VI.

## II. TIME-DELAY MODEL OF OFB

### A. Boundary Conditions in the Laser Cavity Under OFB

The present model of semiconductor lasers under OFB is schematically illustrated in Fig. 1. By supposing  $l$  to be the distance from the laser front facet to the external mirror,  $n_{r2}$  to be the refractive index of the external cavity, and  $c$  as the speed of light in vacuum, the feedback light has a time delay of

$$\tau = \frac{2n_{r2}l}{c}. \quad (1)$$

The electric components of the optical fields in the laser cavity, i.e., in the solitary laser, and the external cavity along the  $z$  direction are assumed as

$$E_1(z, t) = [A_1(z, t) + B_1(z, t)]e^{j\omega t} + c.c., \quad \text{for } 0 \leq z \leq L \quad (2)$$

$$E_2(z, t) = [A_2(z, t) + B_2(z, t)]e^{j\omega t} + c.c. \quad (3)$$

for  $L \leq z \leq L + l$

where  $A_1$  and  $A_2$  are the forward traveling components of the fields, while  $B_1$  and  $B_2$  are the backward traveling components, respectively.  $L$  is the length of the laser cavity. In the present model, the OFB is counted as the time delay of the laser light at the front facet due to round trips in the external cavity. That

is, the boundary conditions at the back facet ( $z = 0$ ) and front facet ( $z = L$ ) become

$$A_1(0, t) = r_b B_1(0, t) \quad (4)$$

$$B_1(L, t) = r_1 T A_1(L, t) \quad (5)$$

$$A_2(L, t) = t_{12} X A_1(L, t) \quad (6)$$

where the function  $T$  determines the amount of the feedback due to time delay in the external cavity and is determined by

$$T = 1 + \frac{t_{12}t_{21}}{r_1} \sum_{m=1}^{\infty} r_{\text{ex}}^m t_2^{m-1} e^{-jm\omega\tau} \frac{A_1(L, t - m\tau)}{A_1(L, t)} \equiv |T|e^{-j\varphi} \quad (7)$$

and the transmission function  $X$  is given by

$$X = 1 + \sum_{m=0}^{\infty} r_2^m r_{\text{ex}}^m e^{-jm\omega\tau} \frac{A_1(L, t - m\tau)}{A_1(L, t)}. \quad (8)$$

Here, the index  $m$  counts the round trips in the external cavity,  $t_{12}$  and  $t_{21}$  are the transmission coefficients at the front facet from the laser cavity to the external cavity, and from the external cavity to the laser cavity, respectively,  $r_b$  is the reflection coefficient at the back facet,  $r_1$  and  $r_2$  are the reflection coefficients at the front facet from the sides of the laser cavity and the external cavity, respectively, and  $r_{\text{ex}}$  is the reflection coefficient at the external mirror. The phase  $\varphi$  is defined as delayed phase of the function  $T$  as in (7), and is very important to determine the lasing operation. These transmission and reflection coefficients are complex values, in general, and are given with power reflection coefficients of  $R_b$ ,  $R_f$ , and  $R_{\text{ex}}$  and phase changes such as

$$r_1 = \sqrt{R_f} e^{-j\phi_1} \quad (9)$$

$$r_2 = \sqrt{R_f} e^{-j\phi_2} \quad (10)$$

$$r_b = \sqrt{R_b} e^{-j\phi_b} \quad (11)$$

$$r_{\text{ex}} = \sqrt{R_{\text{ex}}} e^{-j\phi_{\text{ex}}} \quad (12)$$

$$t_{21} = \frac{n_{r1}}{n_{r2}} \sqrt{1 - R_f} e^{-j\phi_t} \quad (13)$$

$$t_{12} = \frac{n_{r2}}{n_{r1}} \sqrt{1 - R_f} e^{-j\phi_t} \quad (14)$$

with the phase relation of

$$\phi_1 + \phi_2 - 2\phi_t = \pm\pi. \quad (15)$$

### B. Threshold and Phase Conditions Under OFB

By substituting the definitions of the forward and backward components of the field in the laser cavity

$$A_1(z, t) = A_1(0, t) e^{\{(g-\kappa)z/2 - j\beta_1 z\}} \quad (16)$$

$$B_1(z, t) = B_1(L, t) e^{\{(g-\kappa)(L-z)/2 - j\beta_1(L-z)\}} \quad (17)$$

with  $g$ ,  $\kappa$ , and  $\beta_1$  as the gain coefficient, the internal loss, and the propagation constant in the laser cavity, respectively, the oscillation condition of the lasers under the OFB becomes

$$1 = \sqrt{R_f R_b} |T| \exp\{(g - \kappa)L\} \times \exp\{-j[2\beta_1 L + \phi_1 + \phi_b + \varphi]\} \quad (18)$$

and is separated to the following gain and phase conditions:

$$G_{\text{th}} = G_{\text{th0}} + \frac{c}{n_{r1}L} \ln \frac{1}{|T|} \quad (19)$$

$$2\beta_1 L + \phi_b + \phi_1 + \varphi = 2s\pi \quad (20)$$

where  $s$  is an integer.  $G_{\text{th0}}$  is threshold gain in the solitary laser and is defined by

$$G_{\text{th0}} = \frac{c}{n_{r1}} \left[ \kappa + \frac{1}{2L} \ln \frac{1}{R_f R_b} \right]. \quad (21)$$

### C. Modified Rate Equations

In this subsection, we follow the procedures given in [28] and [29] to show how the rate equations in a solitary laser are modified when the laser is subjected to the OFB. The electric field  $E(r, t)$  in the solitary laser is expressed in terms of a slowly time-varying amplitude  $\tilde{E}(t)$ , and the oscillating frequency  $\omega$  as

$$E(r, t) = \tilde{E}(t)\Phi(r)e^{j\omega t} + \text{c.c.} \quad (22)$$

where  $\Phi(r)$  is the spatial field distribution of the field whose value is normalized in the solitary laser. The frequency  $\omega$  is defined for the operation without OFB. By substituting this expression in Maxwell's equations, the following equation of the amplitude  $\tilde{E}(t)$  is obtained:

$$\frac{\partial \tilde{E}}{\partial t} = \frac{1}{2} \left\{ G - G_{\text{th0}} + j\Psi + \frac{c}{n_{r1}L} \ln T \right\} \tilde{E}. \quad (23)$$

Here,  $G$  is the optical gain and is defined to include the nonlinear gain suppression effect as [30], [31]

$$G = A - B \frac{2\varepsilon_0 n_{r1}^2}{\hbar\omega} |\tilde{E}|^2 \quad (24)$$

where

$$A = \frac{a\xi}{V}(N - N_g) \quad (25)$$

is the linear gain coefficient with  $N$  as the number of injected electrons,  $a$  and  $N_g$  are material constants, and  $\xi$  is the field confinement factor in the active region of volume  $V$ .  $B$  is the nonlinear gain coefficient. The coefficient  $\Psi$  determines the phase change due to the simulated emission and is defined in the solitary laser by [29]

$$\Psi = \frac{\alpha a \xi}{V}(N - \bar{N}) \quad (26)$$

where  $\alpha$  is the so-called linewidth enhancement factor, and  $\bar{N}$  is the time-averaged value of  $N$  without feedback. The function  $T$  and  $X$  defined in (7) and (8) are rewritten with substitutions of (9)–(15) as

$$\begin{aligned} T &= 1 - \frac{1 - R_f}{R_f} \sum_{m=1}^{\infty} (R_{\text{ex}} R_f)^{m/2} e^{-jm\psi} \frac{\tilde{E}(t - m\tau)}{\tilde{E}(t)} \\ &= |T| e^{-j\varphi} \end{aligned} \quad (27)$$

$$X = 1 + \sum_{m=0}^{\infty} (R_{\text{ex}} R_f)^{m/2} e^{-jm\psi} \frac{\tilde{E}(t - m\tau)}{\tilde{E}(t)} \quad (28)$$

where

$$\psi = \phi_2 + \phi_{\text{ex}} + \omega\tau \quad (29)$$

represents the phase difference between the delayed injected field and the reflected field in the laser cavity at the front facet. The phase  $\varphi$  in the function  $T$  is obviously given by

$$\varphi = -\tan^{-1} \frac{\Im T}{\Re T} + f\pi \quad (30)$$

where  $f$  is an integer.

Equation (27) is applicable for an arbitrary amount of OFB. The so-called Lang and Kobayashi model [15] is obtained from (27) by supposing weak OFB with  $R_{\text{ex}} \ll R_f$  and a constant phase due to the round trip of time delay  $\tau$ , such that we get

$$\ln T \approx -(1 - R_f) \sqrt{\frac{R_{\text{ex}}}{R_f}} e^{-j\omega\tau} \left| \frac{\tilde{E}(t - \tau)}{\tilde{E}(t)} \right| \quad \text{for } R_{\text{ex}} \ll R_f.$$

We proceed with our analysis in this paper based on (27).

The dynamic (23) can be transformed to a couple of equations for the photon number  $S(t)$  and the phase  $\theta(t)$  by writing the complex field amplitude  $\tilde{E}(t)$  with the phase term  $\theta(t)$  as

$$\tilde{E}(t) = |\tilde{E}(t)| e^{j\theta(t)} \quad (31)$$

and transforming  $|\tilde{E}(t)|$  to  $S(t)$  using the relation [32]

$$\frac{2\varepsilon}{\hbar\omega} |\tilde{E}|^2 = \begin{cases} S + 1, & \text{for optical emission} \\ S, & \text{for optical absorption.} \end{cases} \quad (32)$$

Therefore, the following rate equations are obtained:

$$\frac{dS}{dt} = \left\{ \frac{a\xi}{V}(N - N_g) - \text{BS} - G_{\text{th0}} + \frac{c}{n_{r1}L} \ln |T| \right\} S + \frac{a\xi}{V} N \quad (33)$$

$$\frac{d\theta}{dt} = \frac{\alpha a \xi}{2V}(N - \bar{N}) - \frac{c}{2n_{r1}L}(\varphi - \bar{\varphi}). \quad (34)$$

The last term in (33) represents inclusion of the spontaneous emission. The functions  $T$  and  $X$  are then given in terms of  $S$  by

$$\begin{aligned} T &= 1 - \frac{1 - R_f}{R_f} \sum_{m=1}^{\infty} (R_f R_{\text{ex}})^{m/2} \\ &\quad \times e^{-jm\psi} \sqrt{\frac{S(t - m\tau)}{S(t)}} \frac{e^{j\theta(t - m\tau)}}{e^{j\theta(t)}} \end{aligned} \quad (35)$$

$$\begin{aligned} X &= 1 + \sum_{m=0}^{\infty} (R_{\text{ex}} R_f)^{m/2} \\ &\quad \times e^{-jm\psi} \sqrt{\frac{S(t - m\tau)}{S(t)}} \frac{e^{j\theta(t - m\tau)}}{e^{j\theta(t)}}. \end{aligned} \quad (36)$$

The variable  $\bar{\varphi}$  is a time-averaged value of  $\varphi$ . The nonlinear gain coefficient is given by [30], [32]

$$B = \frac{9\hbar\omega}{4\varepsilon_0 n_{r1}^2} \left( \frac{\tau_{\text{in}}}{\hbar} \right)^2 \left( \frac{\xi}{V} \right)^2 a |R_{cv}|^2 (N - N_s) \quad (37)$$

where  $R_{cv}$  is the dipole moment,  $\tau_{\text{in}}$  is the intraband relaxation time,  $N_s$  is an injection level characterizing the saturation coefficient,  $\varepsilon_0$  is the dielectric constant in free space, and  $\hbar$  is the reduced Plank's constant.

The rate equations (33) and (34) of  $S(t)$  and  $\theta(t)$ , with the following equation for the number of injected electrons  $N$ , describe the dynamics of semiconductor lasers subjected to OFB:

$$\frac{dN}{dt} = -\frac{a\xi}{V}(N - N_g)S - \frac{N}{\tau_s} + \frac{I}{e} \quad (38)$$

where  $I$  is the injection current,  $\tau_s$  is the electron lifetime by the spontaneous emission, and  $e$  is the electron charge.

### D. Emitted Power From the Back Facet and the External Mirror

By going back to the propagating field expressions in (2) and (3), we should determine equations for output powers from the

back facet  $P_b$  and the external mirror  $P_{ex}$ . The electric field components are related with the component  $A_1(L)$  at the front facet as

$$A_1(0) = A_1(L)e^{-(g-\kappa)L/2} \quad (39)$$

$$B_1(0) = \frac{e^{j\phi_b}}{\sqrt{R_b}} A_1(L)e^{-(g-\kappa)L/2} \quad (40)$$

$$B_1(L) = \sqrt{R_f} e^{-j\phi_1} T A_1(L) \quad (41)$$

$$A_2(L) = \sqrt{\frac{n_{r2}}{n_{r1}}} (1 - R_f) e^{-j\phi_1} X A_1(L) \quad (42)$$

$$A_2(L + \ell) = \sqrt{\frac{n_{r2}}{n_{r1}}} (1 - R_f) e^{-j\phi_1} X e^{-j\beta_2 \ell} A_1(L) \quad (43)$$

$$B_2(L) = \sqrt{\frac{n_{r2}}{n_{r1}}} (1 - R_f) e^{-j\phi_1} X e^{-j[\beta_1 + \beta_2]\ell} \times \sqrt{R_g} e^{-\phi_g} A_1(L) \quad (44)$$

$$B_2(L + \ell) = \sqrt{\frac{n_{r2}}{n_{r1}}} (1 - R_f) e^{-j\phi_1} X e^{-j\beta_2 \ell} \times \sqrt{R_g} e^{-\phi_g} A_1(L) \quad (45)$$

where the functions  $T$  and  $X$  are defined in this description as given in (35) and (36), and  $\beta_2$  is the propagation constant in the external cavity.

The number of photons contained in the laser cavity  $S$  and the external cavity  $S_{ex}$  are given with  $A_1(L)$  as

$$S = \frac{2L}{\hbar\omega} \frac{1 + [1/\sqrt{R_b} - \sqrt{R_b}]\sqrt{R_f}|T| - |T|^2 R_f}{(1/2) \ln(1/R_f R_b) + \ln(1/|T|)} \times |A_1(L)|^2 \quad (46)$$

$$S_{ex} = \frac{n_{r2}}{n_{r1}} \frac{\ell}{L} (1 + R_{ex})(1 - R_f) \times \frac{1/2 \ln 1/R_f R_b + \ln 1/|T|}{1 + [1/\sqrt{R_b} - \sqrt{R_b}]\sqrt{R_f}|T| - |T|^2 R_f} |X|^2 S. \quad (47)$$

The power emitted from the back facet  $P_b$  and the external mirror  $P_{ex}$  are then given by

$$P_b = \{1 - R_b\} \sqrt{\frac{R_f}{R_b}} \frac{(1/2) \ln(1/R_f R_b) + \ln(1/|T|)}{1 + [1/\sqrt{R_b} - \sqrt{R_b}]\sqrt{R_f}|T| - |T|^2 R_f} \times |T| \frac{\hbar\omega c}{2n_{r1} L} S \quad (48)$$

$$P_{ex} = \frac{\hbar\omega c}{2n_{r2} L} \frac{n_{r2}}{n_{r1}} (1 - R_{ex})(1 - R_f) \times \frac{(1/2) \ln(1/R_f R_b) + \ln(1/|T|)}{1 + [1/\sqrt{R_b} - \sqrt{R_b}]\sqrt{R_f}|T| - |T|^2 R_f} |X|^2 S. \quad (49)$$

### III. PROCEDURES OF NUMERICAL SIMULATIONS

The present model is applied to simulate the dynamics and identify the operation of semiconductor lasers under OFB. The simulation was performed by numerical integration of the rate equations (33), (34), and (38) with the fourth-order Runge–Kutta method. The laser system of InGaAs emitting in a wavelength of 980 nm was counted in the simulation. Typical numerical values of this laser are listed in Table I. The external cavity was assumed to consist of an optical fiber of refractive index  $n_{r2} = 1.5$ . The length of the external cavity was fixed at 1.0 m. The time step of integration was set as  $\Delta t = 5$  ps, which is so small that the cutoff frequency of the

TABLE I  
VALUES OF PARAMETERS OF 980-nm InGaAs LASERS AND SYSTEM CONFIGURATIONS USED IN THE PRESENT COMPUTER SIMULATION

Symbol	Parameter	Value	Unit
$a$	Tangential parameter of linear gain	$2.21 \times 10^{-12}$	$\text{m}^3 \text{s}^{-1}$
$N_g$	Electron number at transparency	$4.08 \times 10^8$	--
$R_{cv}^2$	Square value of the dipole moment	$2.8 \times 10^{-57}$	$\text{C}^2 \text{m}^2$
$N_s$	Value of the electron number	$1.53 \times 10^8$	--
	characterizing the nonlinear gain		
$\tau_{in}$	Intraband relaxation time	0.1	ps
$\tau_s$	Electron lifetime	2.79	ns
$\alpha$	Linewidth enhancement factor	2	--
$n_{r1}$	Refractive index of active region	3.5	--
$n_{r2}$	Refractive index of external region	1.5	--
$L$	Length of the active region	800	$\mu\text{m}$
$\ell$	Length of the external cavity	1	m
$V$	Volume of the active region	400	$\mu\text{m}^3$
$\xi$	Field confinement factor	0.1	--
$R_f$	Reflectivity at front facet	0.02	--
$R_b$	Reflectivity at back facet	0.98	--

Fourier transform of the laser signal is much higher than both the relaxation frequency  $f_r$  and the external cavity frequency  $f_{ex}$ . The integration was carried out over a period of 10  $\mu\text{s}$ , for which time of the operation reaches steady state. Investigations of laser operation and dynamics were done over wide ranges of the OFB, ranging from  $R_{ex}/R_f = 10^{-5}$ –50 and injection current from  $I/I_{th0} = 1$ –10, where  $I_{th0}$  is the threshold current of the solitary laser. The integration was first made without OFB, i.e., putting  $R_{ex} = 0$  and  $\varphi = 0$  in (36) and (37), from time  $t = 0$  until the round trip time  $\tau$ . The dc values  $\bar{S}$  and  $\bar{N}$  of the photon number  $S(t)$  and the electron number  $N(t)$  are determined from the steady-state solutions of the solitary rate equations as

$$\bar{S} = \frac{I - I_{th0}}{eG_{th0}} \quad (50)$$

$$\bar{N} = \left[ \frac{N_{th} + \frac{V}{a\xi} B\bar{S}}{\bar{S} + 1} \right] \bar{S}. \quad (51)$$

The calculated values of  $S$  and  $\theta$  were then stored for use as time-delayed values  $S(t-\tau)$  and  $\theta(t-\tau)$  for the further integration of the rate equations (33), (34), and (38), including the feedback terms. However, the simulation results of the time-varying output power were found to be insensitive to the variation of  $\psi$  in the present case of long external cavity. The choice of  $\psi$  may be critical to decide the optimum operating conditions for stable operation of lasers in the cases of short external cavities [5]. The phase  $\varphi$  of the feedback light was determined with (30), where

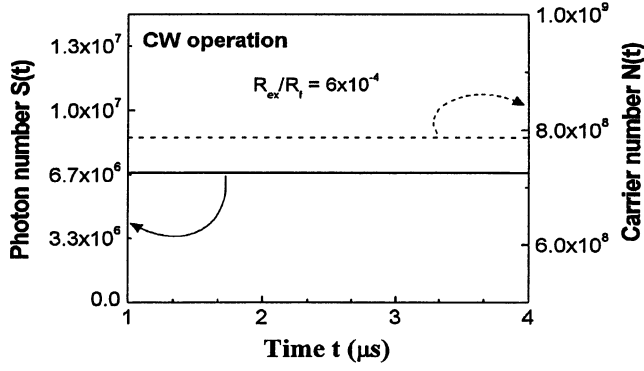


Fig. 2. Simulation result of CW operation of lasers when  $R_{ex}/R_f = 6 \times 10^{-4}$ , and  $I = 6I_{th}$ : time variation of the photon number  $S(t)$  and carrier number  $N(t)$ . Both  $S$  and  $N$  attain constant values.

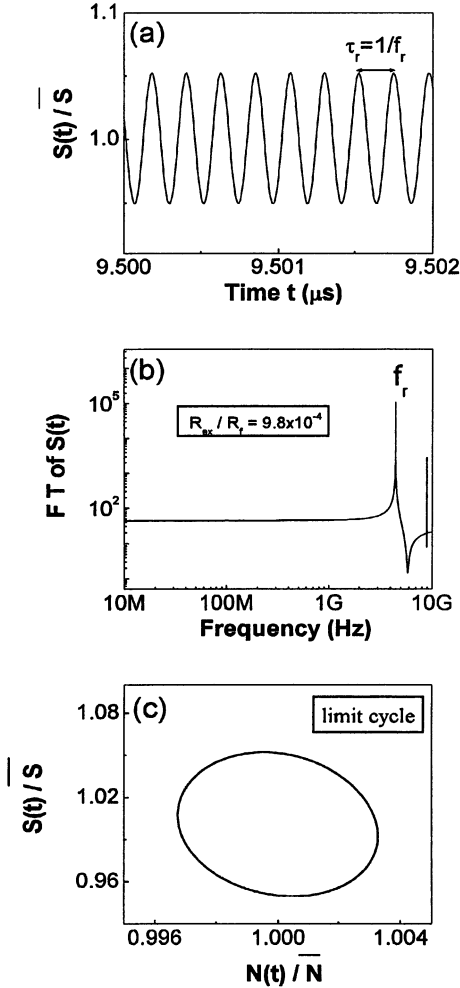


Fig. 3. An example of simulation results of uniform pulsation of lasers in the moderate OFB regime when  $R_{ex}/R_f = 9.8 \times 10^{-4}$ . (a) Time variation of the photon number. (b) Frequency spectrum of the FT. (c) Phase portrait. The laser operates in uniform pulsation in the relaxation frequency  $f_r$ .

the integer  $f$  was chosen to vary  $\varphi$  continuously for time evolution, because the solution of arc tangent is limited in the range of  $-\pi/2$  to  $\pi/2$  in the computer work. The averaged values  $\bar{\varphi}$  is set to zero in the present calculations.

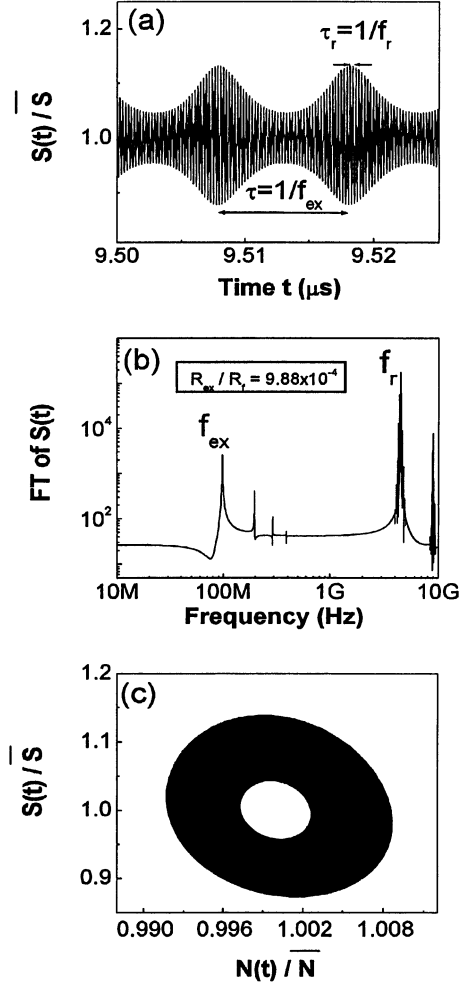


Fig. 4. Example of simulation results of beating pulsation of lasers in the regime of moderate OFB when  $R_{ex}/R_f = 9.88 \times 10^{-4}$ . (a) Time variation of the photon number. (b) Frequency spectrum of the FT. (c) Phase portrait. Pulsation in the relaxation frequency  $f_r$  is seen and is enveloped by pulsation in the external frequency  $f_{ex}$ .

#### IV. THEORETICAL RESULTS AND DISCUSSIONS

##### A. Variation of the Laser Operation With OFB

Various operating states are shown in Figs. 2–7. The injection current level and the OFB phase difference were set as  $I = 6.0I_{th}$  and  $\psi = \omega\tau$  for all cases. The corresponding threshold current levels were determined from the light versus current (L-I) characteristics as will be shown in Fig. 8 [where L here means the time-averaged value of the photon number  $S(t)$ ]. The photon number is normalized by its timely averaged values  $\bar{S}$ . Fig. 2 is the case with very weak OFB corresponding to external reflectivity of  $R_{ex}/R_f = 6.0 \times 10^{-4}$  with  $I_{th} = 45.1$  mA. The figure plots the time variation of the photon number  $S(t)$  and the carrier number  $N(t)$ , and indicates that both  $S(t)$  and  $N(t)$  attain constant values, which represents CW operation.

Fig. 3 represents the case of external reflectivity of  $R_{ex}/R_f = 9.8 \times 10^{-4}$  with  $I_{th} = 45.09$  mA, while in Fig. 4,  $R_{ex}/R_f = 9.88 \times 10^{-4}$  with  $I_{th} = 45.089$  mA. In Fig. 5,  $R_{ex}/R_f = 1.0 \times 10^{-3}$  with  $I_{th} = 45.087$  mA. In these figures,

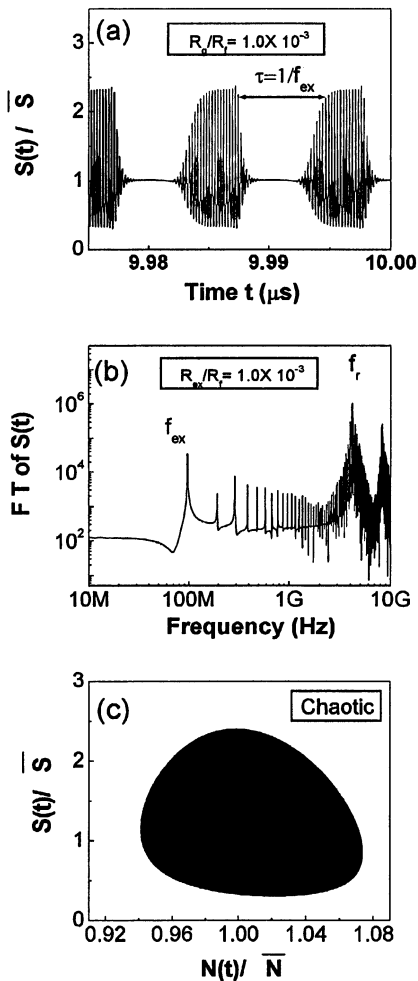


Fig. 5. Example of simulation results of the laser output in the regime of moderate OFB when  $R_{ex}/R_f = 1 \times 10^{-3}$ . (a) Time variation of the photon number. (b) Frequency spectrum of the FT. (c) Phase portrait. Random variation of the photon number is seen in (a) with broadened peaks at the external frequency  $f_{ex}$  and the relaxation frequency  $f_r$  in (b). The phase portrait indicates a chaotic attractor.

part (a) shows the time variation of the photon number  $S(t)$ , (b) shows the frequency spectrum of the photon number  $S(t)$  due to Fourier transform (FT) calculation, and (c) shows the attractor trace between the photon number  $S(t)$  and carrier number  $N(t)$ . As found in Fig. 3, the laser shows a weak and uniform pulsation with the relaxation frequency  $f_r = 4.44$  GHz when the OFB increases a little bit beyond the CW operation.

By increasing the OFB, the laser shows a weak but beating pulsation with the relaxation frequency  $f_r$  and the external cavity frequency  $f_{ex}$ , as shown in Fig. 4. When the OFB reaches  $R_{ex}/R_f = 1.0 \times 10^{-3}$ , operation of the laser becomes more complicated, and could be called chaotic operation [33]–[38]. Fig. 5(a) plots an example of the time variation of the photon number  $S(t)$  in this chaos region. Although the figure shows periodic components of  $S(t)$  in both frequencies  $f_{ex}$  and  $f_r$ ,  $S(t)$  exhibits an irregular pattern. The random variation of  $S(t)$  is seen in Fig. 5(b) as a broadening of those peaks, as well as appearance of peaks with different values at higher harmonics of  $f_{ex}$  and  $f_r$ . This means that the laser operates unstably under two threshold conditions; one corresponds to the

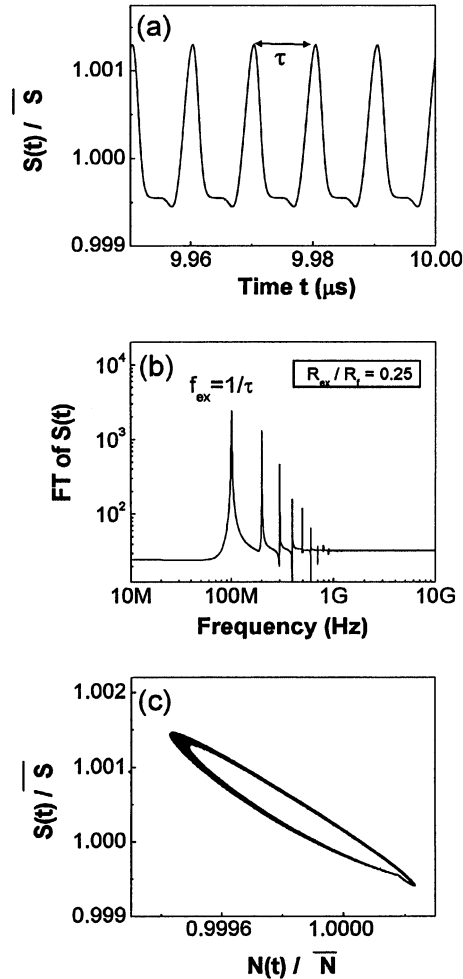


Fig. 6. Example of simulation results of uniform pulsation of lasers in the strong OFB regime when  $R_{ex}/R_f = 0.25$ . (a) Time variation of the photon number. (b) Frequency spectrum of the FT. (c) Phase portrait. The laser operates in uniform pulsation in the external frequency  $f_{ex}$ .

laser cavity, and the other corresponds to the external cavity, which randomize the time variations of both the optical phase  $\theta(t)$  and the electron number  $N(t)$ , and consequently, enhance laser linewidth. The chaotic operation is characterized by a chaotic attractor in the phase diagram, as shown in Fig. 5(c).

Fig. 6 represents an example of pulsing operation in the strong OFB region, which corresponds to  $R_{ex}/R_f = 0.25$  with  $I_{th} = 41.75$  mA. The pulsing frequency in this case is  $f_{ex} = 1/\tau$ , as shown in Fig. 6(a), which plots the time variation of the photon number  $S(t)$ . This result is confirmed by the FT of the photon number in Fig. 6(b). This may mean that the laser is locked at the external cavity frequency  $f_{ex}$ .

In Fig. 7(a), we summarized the laser operation in terms of bifurcation analysis of the temporal peak value of the photon number  $S_{max}(t)$  versus the ratio  $R_{ex}/R_f$ . As the reflectivity ratio  $R_{ex}/R_f$  increases, the laser shows CW operation for sufficiently small  $R_{ex}/R_f$ , starts to show small pulsation with relaxation frequency  $f_r$ , followed by a beating vibration with relaxation frequency  $f_r$  and external cavity frequency  $f_{ex}$ , and then reaches chaotic operation. By increasing  $R_{ex}/R_f$  more than 0.4, the laser changes to CW operation again and reaches stable pulsing operation with the external cavity frequency  $f_{ex}$ .

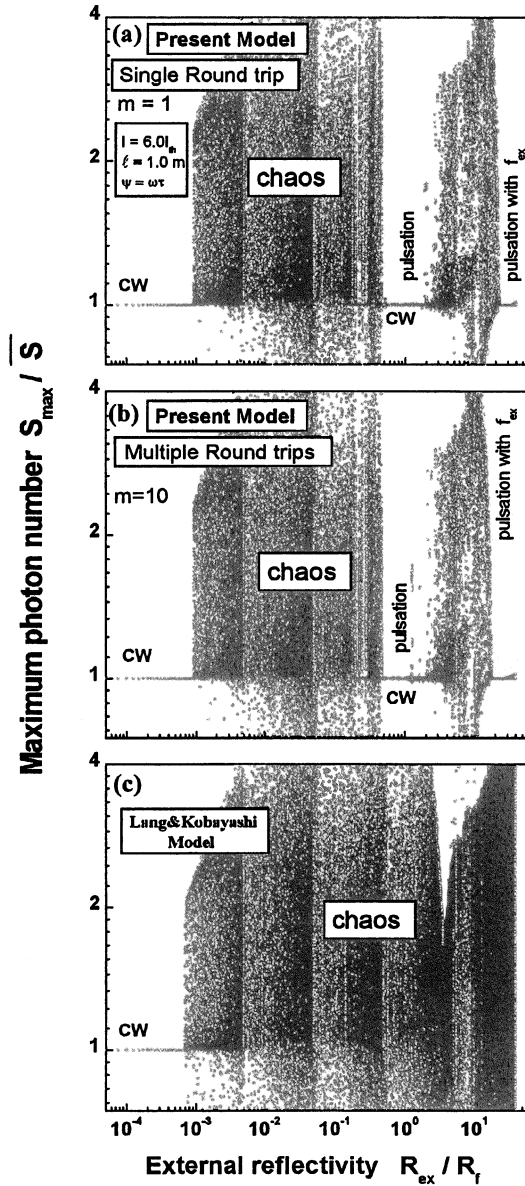


Fig. 7. Summarized diagram for a single-mode semiconductor laser under a wide range of OFB from weak to strong OFB at  $I = 6I_{\text{th}}$ ,  $\ell = 1 \text{ m}$ , and  $\psi = \omega\tau$  in terms of the bifurcation diagram calculated via (a) the present model at single round trip ( $m = 1$ ), (b) the present model at multiples round trips ( $m = 10$ ), and (c) Lang and Kobayashi model. Laser mainly operates in CW under very weak OFB, chaos under moderate OFB, and pulsation in the strong regime of OFB. Under strong OFB Lang and Kobayashi model predicts much irregular pattern of  $S(t)$  deviating strongly from those obtained via our model.

However, the laser enters an instability regime (chaotic operation) as the feedback is further increased to  $R_{\text{ex}}/R_f = 2$ . When  $R_{\text{ex}}/R_f$  more than 20, the laser shows CW operation and pulsing operation with  $f_{\text{ex}}$  again. In such calculations, the round trips between the front facet and external mirror were limited to a single round trip ( $m = 1$ ), which is effective for the case of small reflectivity at the front facet (e.g., AR-coated facet) [26], [27]. Nevertheless, we compare the results in Fig. 7(a) with those obtained by counting ten round trips ( $m = 10$ ), which are plotted in Fig. 7(b). Results in both figures are in good coincidence. Therefore, the multiple round trips time delay can be ignored in the present calculations.

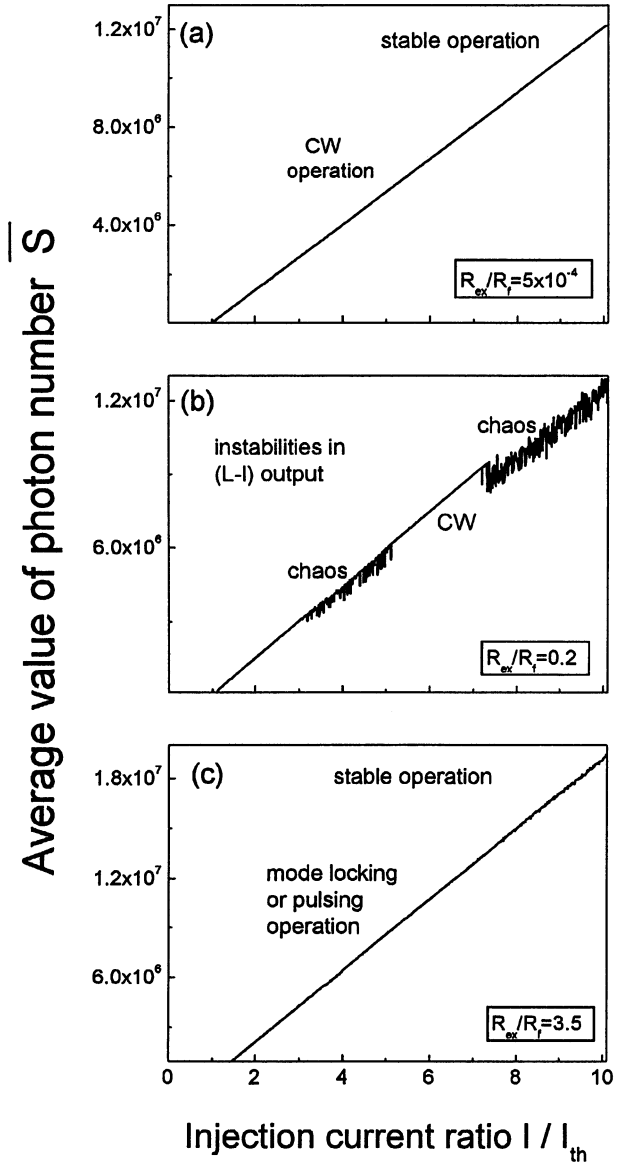


Fig. 8. L-I characteristics of a semiconductor laser under three amounts of OFB. (a)  $R_{\text{ex}}/R_f = 5 \times 10^{-4}$ . (b)  $R_{\text{ex}}/R_f = 0.2$ . (c)  $R_{\text{ex}}/R_f = 3.5$ . Output is smooth and linear under CW and pulsing operation, but has strong nonlinearities under the chaotic operation.

We, moreover, are interested in comparing the results in Fig. 7(a) with those predicted by the Lang and Kobayashi model [15], which is commonly applied to analyze dynamics under OFB. The obtained results are plotted in Fig. 7(c). As shown, the Lang and Kobayashi model predicts similar characteristics up to  $R_{\text{ex}}/R_f = 10^{-3}$ . Above this feedback level, such a model leads to results strongly deviating from the present results. For example, the regions of CW and pulsation operations shown in Fig. 7(a) over  $0.4 < R_{\text{ex}}/R_f < 2.0$  and  $20 < R_{\text{ex}}/R_f$  completely disappear in Fig. 7(c), and the model indicates chaotic dynamics at stronger OFB. That is, the accuracy of applying the Lang and Kobayashi model deteriorates in the range of strong OFB in this case of long cavity.

### B. L-I Characteristics

The operation of the laser also changes with the injection current level. Fig. 8 plots the calculated L-I characteristics under

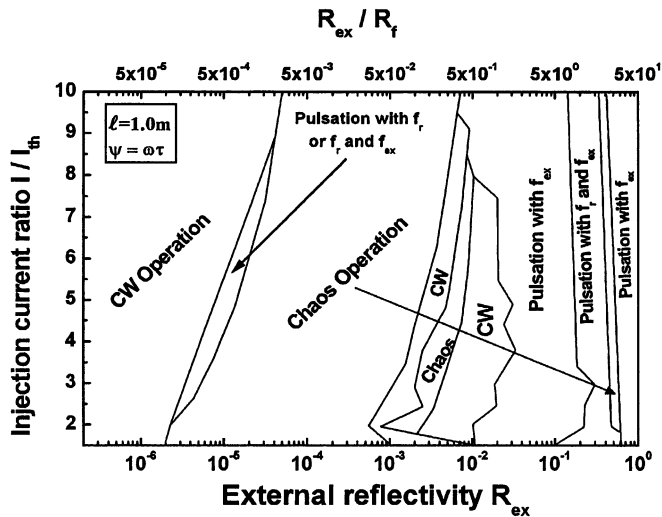


Fig. 9. Classification of operation of semiconductor lasers in terms of  $R_{ex}/R_f$  (from weak to strong OFB) and the injection current. Four possible operations for semiconductor lasers are found: CW, uniform pulsation with frequency  $f_r$ , chaos, and pulsation in the external cavity frequency  $f_{ex}$ . Pulsing operation occupies the regime of strong OFB over the entire range of the current.

three values of the external reflectivity  $R_{ex}/R_f = 5.0 \times 10^{-4}$  corresponding to weak OFB,  $R_{ex}/R_f = 0.2$  corresponding to moderate OFB, and  $R_{ex}/R_f = 3.5$  corresponding to strong OFB. Under weak OFB, the CW operation is identified with straight L-I characteristics in the entire range of the injection current  $I$  without kinks or nonlinearities, as shown in Fig. 8(a). On the contrary, the L-I characteristics shown in Fig. 8(b) exhibit strong instabilities or nonlinearities in the intermediate and high ranges of the injection current, which corresponds with chaotic operations. The smooth variation of the output power with the current corresponds with stable CW operations. Under strong OFB, the operation is pulsing, which is characterized with almost smooth linear L-I characteristics, as shown in Fig. 8(c).

### C. Classification of Laser Operation in Terms of the OFB and Injection Current

The range of operation of InGaAs lasers was classified in a diagram between the injection current ratio  $I/I_{th}$  and the external reflectivity ratio  $R_{ex}/R_f$ , as shown in Fig. 9. As shown in the figure, the laser operates in CW at very weak OFB over the entire range of the injection current  $I$ . Two other regions of CW operation are found at relatively strong OFB over most ranges of  $I$ . The operating region of chaos occupies the region of moderate OFB, while another region is found on a narrow range of strong OFB  $R_{ex}/R_f = 25-30$ . The pulsing operation occupies the region of strong OFB,  $R_{ex}/R_f \geq 3$ , with a narrow region of chaotic operation. A detailed characterization of laser dynamics and operation of lasers operating under strong OFB, which is presented in Fig. 9, is important to understanding the operation of pumping lasers in fiber amplifiers.

## V. EXPERIMENTAL OBSERVATIONS

### A. Experimental Setup

We also investigated the operation characteristics of lasers in the region of strong OFB. The experimental setup is illustrated

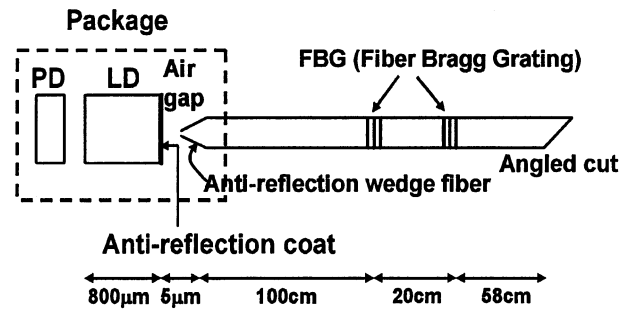


Fig. 10. Experimental set up and illustration of the InGaAs laser, which is connected to a fiber having two FBGs.

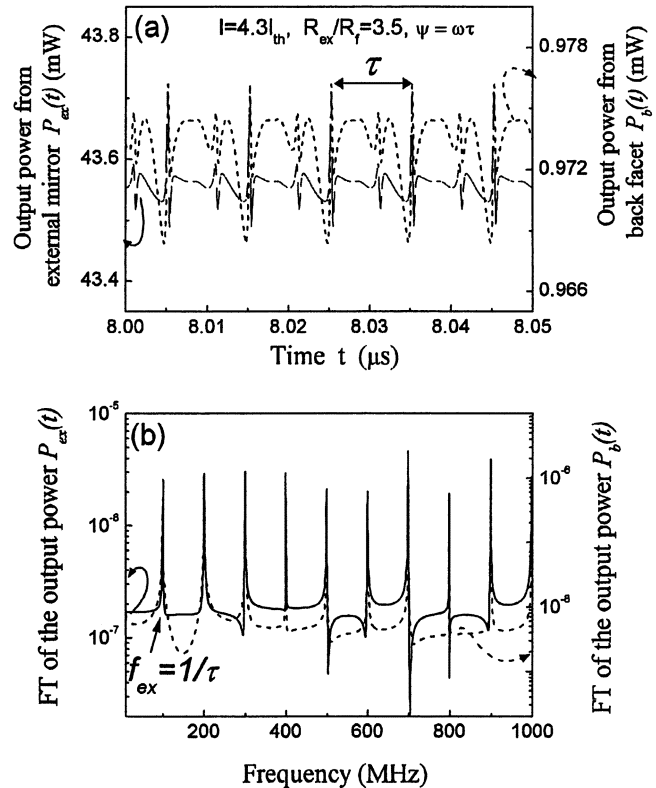


Fig. 11. Simulation results under very strong OFB for  $R_{ex}/R_f = 3.5$ ,  $I = 4.3I_{th}$ ,  $l = 1$  m, and  $\psi = \omega_0\tau$ . (a) Temporal variation of the power emitted from the external mirror  $P_{ex}(t)$  and the back facet  $P_b(t)$ . (b) Frequency spectra of the corresponding FTs. Simulated pulsing operation of the laser is similar to the experimental observations. Laser is stimulated to operate in pulsation.

in Fig. 10. An InGaAs laser was connected to a fiber having two FBGs of central reflectivity  $R_{ex}/R_f = 3.5$  and  $R_{ex2}/R_f = 1$ , and at distances of  $l = 1.0$  m from the laser facet and  $l_2 = 0.2$  m from the first fiber grating, where  $R_f = 0.02$  and  $R_{ex2}$  is the power reflectivity of the second fiber grating. The end of the optical fiber was cut with a tilted angle to avoid additional reflection from the end of the fiber. The output power was obtained from this angle edge. The spectral characteristics of the pulsation were examined by using a spectrum analyzer. The characteristics of the time variations of the photon and the carrier were examined by using a sampling oscilloscope. The variations of the photon number were examined through the output current of an avalanche photodiode (APD). We examined the variation of the output voltage of the laser and assumed it to correspond to the variation of the carrier density.

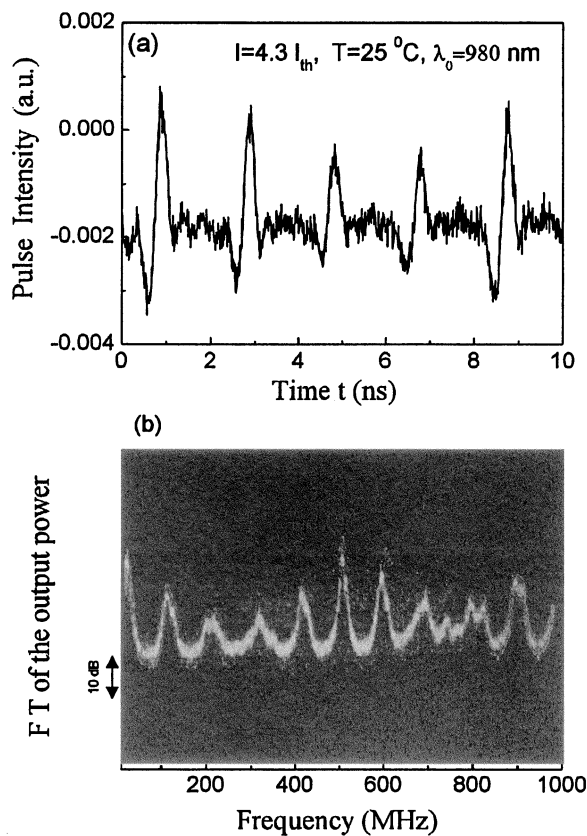


Fig. 12. Observed output characteristics under very strong OFB for  $R_{ex}/R_f = 3.5$ ,  $I = 4.3I_{th}$ ,  $\ell = 1$  m. (a) Temporal variation of the output power from the external mirror. (b) Frequency spectrum of the corresponding FT. Output power exhibits pulsation in the external frequency  $f_{ex}$ . Experimental observation of pulsing output is similar to the simulated results.

### B. Simulated and Observed Pulsing Operations Under Strong OFB

Fig. 11 shows the theoretical result based on our simulation model with one reflecting point of reflectivity  $R_{ex}$ . The operating conditions were assumed as  $I = 4.3I_{th}$ ,  $\psi = \omega\tau$ , and  $R_{ex} = 3.5R_f$  with  $I_{th} = 34.6$  mA. Fig. 11(a) plots the time variations of the power emitted from both the external mirror  $P_{ex}(t)$  and the back facet  $P_b(t)$ , while Fig. 11(b) plots the frequency spectrum of the corresponding FTs.

Typical measured characteristics of the output power of InGaAs lasers subjected to strong OFB is shown in Fig. 12. The results correspond to a high injection current of  $I = 4.3I_{th}$ , where  $I_{th} = 34.6$  mA. Fig. 12(a) plots the waveform of the power emitted from the grating measured by a sampling oscilloscope, while Fig. 12(b) plots the frequency spectrum of the corresponding FT measured by a spectrum analyzer. The observed results shown in Fig. 12(a) indicate pulsing operation of the laser under strong OFB, which is similar to simulated results shown in Fig. 11(a). Moreover, the FT of the emitted power shown in Fig. 12(b) confirms that the pulsing occurs in the external frequency  $f_{ex}$ , as predicted in the simulated results shown in Fig. 11(b). This means that the condition of laser oscillation is mainly determined by the external cavity rather than the laser cavity itself. In conclusion, our model predicts pulsing operation of the laser, corresponding well with the experimental observations.

## VI. CONCLUSION

We proposed an improved model of analysis of OFB in semiconductor lasers. The model is versatile and is applicable under an arbitrary amount of OFB. The model was applied to newly investigate the operation characteristics of 980 nm InGaAs lasers, which have been recently used as pumping sources for fiber amplifiers, under strong OFB. The operation characteristics were also analyzed over wide ranges of OFB and injection current. The following conclusions can be traced from the obtained results.

- 1) The laser operates in CW under very weak OFB.
- 2) Under weak to intermediate feedback, the laser exhibits chaotic operation.
- 3) Under relatively strong feedback, the laser operates in either CW or chaos, depending on the magnitude of the injection current.
- 4) Under strong feedback, the laser output is pulsing in the oscillating frequency of the external cavity, which may be a type of frequency locking.
- 5) The L-I characteristics are smooth and linear when the laser operates in CW, but have strong nonlinearities under chaotic operation. In the pulsing region, the L-I characteristics are almost smooth and linear, but have small nonlinearities at high injection currents of  $8I_{th}$ – $10I_{th}$ .

## ACKNOWLEDGMENT

The authors acknowledge Drs. T. Shimiza, A. Kasukawa, T. Yamagachi, Y. Ohki, and N. Hashizame, with the Furukawa Electric Co. LTD, for helpful discussions.

## REFERENCES

- [1] G. P. Agrawal and N. K. Dutta, *Semiconductor Lasers*, 2nd ed. New York: Van Nostrand, 1993.
- [2] K. Petermann, *Laser Diode Modulation and Noise*. Boston, MA: Kluwer, 1991.
- [3] D. Lenstra, B. H. Verbeek, and A. J. den Boef, "Coherence collapse in single-mode semiconductor lasers due to optical feedback," *IEEE J. Quantum Electron.*, vol. QE-21, pp. 674–679, June 1985.
- [4] R. W. Tkach and A. R. Chraplyvy, "Regimes of feedback effects in 1.5- $\mu$ m distributed-feedback lasers," *J. Lightwave Technol.*, vol. LT-4, pp. 1655–1661, Nov. 1986.
- [5] N. Schunk and K. Petermann, "Numerical analysis of the feedback regimes for a single-mode semiconductor laser with external feedback," *IEEE J. Quantum Electron.*, vol. 24, pp. 1242–1247, July 1988.
- [6] B. Tromborg and J. Mork, "Stability analysis and the route to chaos for laser diodes with optical feedback," *IEEE Photon. Technol. Lett.*, vol. 2, pp. 549–552, Aug. 1990.
- [7] J. Mork, J. Mark, and B. Tromborg, "Route to chaos and competition between relaxation oscillations for a semiconductor laser with optical feedback," *Phys. Rev. Lett.*, vol. 65, pp. 1999–2002, Oct. 1990.
- [8] J. Mork, B. Tromborg, and J. Mark, "Chaos in semiconductor laser with optical feedback: Theory and experiment," *IEEE J. Quantum Electron.*, vol. 28, pp. 93–108, Jan. 1992.
- [9] J. McInerney, L. Reekie, and D. J. Bradley, "Observation of bistable optical effects in a twin GaAs/GaAlAs diode external cavity ring laser," *Electron. Lett.*, vol. 20, pp. 586–588, July 1984.
- [10] P. Zorabedian, W. R. Trutna, Jr., and L. S. Cutler, "Bistability in grating—Tuned external cavity semiconductor lasers," *IEEE J. Quantum Electron.*, vol. QE-23, pp. 1855–1860, Nov. 1987.
- [11] J. Harrison and A. Mooradian, "Linewidth and offset frequency locking of an external cavity GaAlAs laser," *IEEE J. Quantum Electron.*, vol. 25, pp. 1152–1155, June 1989.
- [12] J. M. Kahn, C. A. Burrus, and G. Raybon, "High-stability 1.5  $\mu$ m external-cavity semiconductor lasers for phase lock applications," *IEEE Photon. Technol. Lett.*, vol. 1, pp. 159–161, July 1989.

- [13] G. Wenke, R. Gross, P. Meissner, and E. Patzak, "Characteristics of a compact three-cavity laser configuration," *J. Lightwave Technol.*, vol. LT-5, pp. 608–615, Apr. 1987.
- [14] G. P. Agrawal and C. H. Henry, "Modulation performance of a semiconductor laser coupled to an external high-Q resonator," *IEEE J. Quantum Electron.*, vol. 24, pp. 134–142, Feb. 1988.
- [15] R. Lang and K. Kobayashi, "External optical feedback effects on semiconductor injection laser properties," *IEEE J. Quantum Electron.*, vol. QE-16, pp. 347–355, Mar. 1980.
- [16] J. H. Osmundsen and N. Gade, "Influence of optical feedback on laser frequency spectrum and threshold conditions," *IEEE J. Quantum Electron.*, vol. QE-19, pp. 465–469, Mar. 1983.
- [17] J. Sacher, W. Elsasser, and E. O. Gobel, "Nonlinear dynamics of semiconductor laser emission under variable feedback conditions," *IEEE J. Quantum Electron.*, vol. 27, pp. 373–379, Mar. 1991.
- [18] D. R. Hjelme, A. R. Mickelson, and R. G. Beausoleil, "Semiconductor laser stabilization by external optical feedback," *IEEE J. Quantum Electron.*, vol. 27, pp. 352–372, Mar. 1991.
- [19] Y. Cho and T. Umeda, "Observation of chaos in a semiconductor laser with delayed feedback," *Opt. Commun.*, vol. 59, pp. 131–136, Aug. 1986.
- [20] J. Mork, "Nonlinear dynamics and stochastic behavior of semiconductor lasers with optical feedback," Ph.D. dissertation, Tech. Univ. Denmark, Lyngby, Denmark, Aug. 1988.
- [21] T. Mukai and K. Otsuka, "New route to optical chaos: Successive subharmonic oscillation cascade in a semiconductor laser coupled to an external cavity," *Phys. Rev. Lett.*, vol. 55, pp. 1711–1714, Oct. 1985.
- [22] A. Hohl and A. Gavrielides, "Bifurcation cascade in a semiconductor laser subject to optical feedback," *Phys. Rev. Lett.*, vol. 82, pp. 1148–1151, Feb. 1999.
- [23] Y. Kitaoka, H. Sato, K. Mizuchi, K. Yamamoto, and M. Kato, "Intensity noise of laser diodes with optical feedback," *IEEE J. Quantum Electron.*, vol. 32, pp. 822–827, May 1996.
- [24] K. I. Kallimani and M. J. O'Mahony, "Relative intensity noise for laser diodes with arbitrary amounts of optical feedback," *IEEE J. Quantum Electron.*, vol. 34, pp. 1438–1446, Aug. 1998.
- [25] M. Yamada, "Computer simulation of feedback-induced noise in semiconductor lasers operating with self-sustained pulsation," *Trans. IEICE*, vol. E81-C, pp. 768–780, May 1998.
- [26] H. Rong-Qing and T. Shang-Ping, "Improved rate equations for external cavity semiconductor lasers," *IEEE J. Quantum Electron.*, vol. 25, pp. 1580–1584, June 1989.
- [27] L. N. Langley, K. A. Shore, and J. Mork, "Dynamical and noise properties of laser diodes subject to strong optical feedback," *Opt. Lett.*, vol. 19, pp. 2137–2139, Dec. 1994.
- [28] M. Yamada and M. Suhara, "Analysis of excess noise induced by optical feedback in semiconductor lasers based on mode competition theory," *Trans. IEICE*, vol. E-73, pp. 77–82, Jan. 1990.
- [29] M. Ahmed, M. Yamada, and M. Saito, "Numerical modeling of intensity and phase noise in semiconductor lasers," *IEEE J. Quantum Electron.*, vol. 37, pp. 1600–1610, Dec. 2001.
- [30] M. Yamada and Y. Suematsu, "Analysis of gain suppression in undoped injection lasers," *J. Appl. Phys.*, vol. 52, pp. 2653–2664, Apr. 1981.
- [31] M. Ahmed and M. Yamada, "An infinite-order perturbation approach to gain calculation in injection semiconductor lasers," *J. Appl. Phys.*, vol. 84, pp. 3004–3015, Sept. 1998.
- [32] *Handbook of Semiconductor Lasers and Photonic Integrated Circuits*, Chapman & Hall, London, U.K., 1994.
- [33] A. T. Ryan, G. P. Agrawal, G. R. Gray, and E. C. Gage, "Optical-feedback-induced chaos and its control in multimode semiconductor lasers," *IEEE J. Quantum Electron.*, vol. 30, pp. 668–678, Mar. 1994.
- [34] H. G. Winful, Y. C. Chen, and J. M. Liu, "Frequency locking, quasiperiodicity, and chaos in modulated self-pulsing semiconductor lasers," *Appl. Phys. Lett.*, vol. 48, pp. 616–618, Mar. 1986.
- [35] N. Kikuchi, Y. Liu, and J. Ohtsubo, "Chaos control and noise suppression in external-cavity semiconductor lasers," *IEEE J. Quantum Electron.*, vol. 33, pp. 56–65, Jan. 1997.
- [36] Y. Cho and T. Umeda, "Chaos in laser oscillations with delayed feedback: Numerical analysis and observation using semiconductor lasers," in *Proc. 13th Int. Quantum Electronics Conf.*, vol. 1, 1984, pp. 497–498.
- [37] G. C. Dente, P. S. Durkin, K. A. Wilson, and C. E. Moeller, "Chaos in the coherence collapse of semiconductor lasers," *IEEE J. Quantum Electron.*, vol. 24, pp. 2441–2447, Dec. 1988.
- [38] V. Annovazzi-Lodi, S. Donati, and M. Manna, "Chaos and locking in a semiconductor laser due to external injection," *IEEE J. Quantum Electron.*, vol. 30, pp. 1537–1541, July 1994.

**Salah G. Abdurhmann** (S'02) was born in Assiut, Egypt, on September 14, 1972. He received the B.Sc. and M.Sc. degrees in physics from Assiut University, Assiut, Egypt, in 1994 and 1998, respectively. He is currently working toward the Ph.D. degree at the Graduate School of Natural Science and Technology, Kanazawa University, Kanazawa, Japan.

His research interests are in the areas of optoelectronics, and statics and dynamics of semiconductor lasers.

**Moustafa Ahmed** (S'99–M'99) was born in Minia, Egypt, in 1966. He received the B.Sc. and M.Sc. degrees in physics from Minia University, El-Minia, Egypt, in 1988 and 1993, respectively, and the Ph.D.Eng. degree from the Graduate School of Natural Science and Technology, Kanazawa University, Kanazawa, Japan, in 1999.

He is currently a Lecturer in the Physics Department of Minia University. From 2000 to 2002, he was a Visiting Fellow at the Department of Electrical and Electronic Engineering of Kanazawa University, supported by the postdoctoral program of the Japan Society for the Promotion of Science (JSPS). His research interests are in the areas of optoelectronics, and statics and dynamics of semiconductor lasers.

**Takaharu Okamoto** was born in Ishikawa, Japan, on August 10, 1976. He received the B.S. and M.S. degrees in electrical and computer engineering from Kanazawa University, Kanazawa, Japan in 2000 and 2002, respectively.

He is currently with the NTT DATA Corporation, Tokyo, Japan.

**Wataro Ishimori** was born in Ishikawa, Japan, on October 21, 1978. He received the B.S. degree in electrical and computer engineering in 2001 from Kanazawa University, Kanazawa, Japan, where he is currently working toward the M.S. degree.

**Minoru Yamada** (M'82) was born in Yamanashi, Japan, on January 26, 1949. He received the B.S. degree in electrical engineering from Kanazawa University, Kanazawa, Japan, in 1971, and the M.S. and Ph.D. degree in electronics engineering from the Tokyo Institute of Technology, Tokyo, Japan, in 1973 and 1976, respectively.

He joined Kanazawa University in 1976, and is presently a Professor. From 1982 to 1983, he was a Visiting Scientist at Bell Laboratories, Holmdel, NJ. His research interests are in semiconductor injection lasers, semiconductor modulators, and unidirectional optical amplifiers.

Dr. Yamada received the Yonezawa Memorial Prize in 1975, the Paper Reward in 1976, and the Achievement Award in 1978 from the IECE of Japan.